

# MambaRain: Multi-Scale Mamba-Attention Framework for 0-3 Hour Precipitation Nowcasting

Chunlei Shi<sup>1,2</sup>, Cui Wu<sup>3</sup>, Xiang Xu<sup>4</sup>, Hao Li<sup>2</sup>, Ni Fan<sup>5</sup>, Xue Han<sup>1</sup>, Yongchao Feng<sup>6</sup>, Yufeng Zhu<sup>1</sup>, Boyu Liu<sup>1</sup>, Zengliang Zang<sup>7</sup>, Hongbin Wang<sup>8</sup>, Yanlan Yang<sup>1</sup> Dan Niu<sup>1,†</sup>

**Abstract**—Accurate precipitation nowcasting over extended horizons (0-3 hours) is crucial for disaster prevention and real-time decision-making, yet remains a critical challenge. Existing deterministic methods typically focus on shorter periods (0-1 or 0-2 hours) and exhibit rapid performance degradation beyond 90 minutes due to difficulties in capturing long-range spatiotemporal dependencies from radar observations. To address these limitations, we propose MambaRain, a novel multi-scale encoder-decoder framework that integrates Mamba’s linear-complexity long-range temporal modeling with self-attention mechanisms. Our core innovation is a hybrid architecture where Mamba blocks capture global temporal evolution across extended sequences via selective state space mechanisms, while self-attention complements this by explicitly modeling spatial correlations within precipitation fields—a capability absent in Mamba’s sequential processing. This synergy enables comprehensive spatiotemporal modeling, extending the effective forecasting window to 2-3 hours with improved accuracy. Furthermore, we introduce a spectral loss to mitigate blurring effects in chaotic precipitation systems, preserving fine-scale motion details. Unlike previous deterministic approaches that struggle with long-range spatiotemporal dependencies, MambaRain achieves superior performance in 0-3 hour nowcasting, with significant accuracy gains especially in the 2-3 hour range. Extensive experiments on Xinjiang and Southeast China SWAN datasets demonstrate substantial improvements over existing methods in both precision and efficiency. Our project is available at <https://spring-lovely.github.io/MambaRain2025/>.

**Index Terms**—0-3h precipitation nowcasting, mamba, self-attention, DEM data.

## I. INTRODUCTION

PRECIPITATION nowcasting—the generation of high-resolution rainfall intensity forecasts for the upcoming 0–3 hours—plays an indispensable role in weather-dependent decision-making across aviation safety, agricultural planning, flood control, and urban infrastructure management [1], [2], [3], [4], [5], [6], [7]. In China, the increasing frequency and intensity of convective precipitation events driven by climate

change have amplified the demand for reliable extended-horizon forecasts, particularly in topographically complex regions such as Xinjiang and Southeast China where orographic effects strongly modulate rainfall patterns. Despite decades of progress in both numerical weather prediction and data-driven approaches, extending the effective forecasting window beyond 90 minutes while preserving spatial fidelity and computational efficiency remains a fundamental and largely unresolved challenge in operational meteorology [8], [9], [10], [11], [12].

Traditional operational nowcasting systems, including optical flow-based methods (e.g., OptFlow) [13] and variational extrapolation approaches (e.g., Sprog) [14], estimate radar-derived precipitation motion fields and advect them forward in time. While computationally efficient, these methods operate under a linear motion assumption that renders them inherently incapable of representing non-linear phenomena such as convective initiation, dissipation, and cell merging—processes that increasingly dominate precipitation evolution beyond the first 30–60 minutes. The fundamental physical barrier is that precipitation systems are governed by chaotic atmospheric dynamics, where small perturbations in thermodynamic instability or moisture convergence lead to rapidly diverging future states, making purely deterministic extrapolation unreliable at extended lead times.

Deep learning approaches have emerged as powerful alternatives by learning complex spatiotemporal patterns directly from large radar observation archives. ConvRNN-based models, including ConvLSTM [15] and TrajGRU [16], introduced recurrent architectures for sequential radar echo processing, while CNN-Transformer hybrids such as AA-TransUnet [17] and Earthformer [18] leveraged attention mechanisms for richer spatiotemporal feature extraction. More recently, NowcastNet [19] integrated physics-constrained generation for improved structural realism. However, a common failure mode persists across these deterministic approaches: optimization with mean squared error (MSE) loss in the spatial domain causes models to converge toward the *conditional mean* of the inherently multi-modal precipitation distribution, producing over-smoothed, blurry predictions at longer lead times where forecast uncertainty is high. This regression-to-the-mean effect becomes increasingly severe beyond the 90-minute mark, rendering forecasts meteorologically unrealistic and operationally misleading—particularly for high-intensity convective events that matter most for hazard warnings.

To mitigate the blurring problem, generative approaches have been applied to precipitation nowcasting. Diffusion-

This work was supported by the Heavy Rainfall Research Foundation of China (No. BYKJ2025M14), China Meteorological Administration Xiong’an Atmospheric Boundary Layer Key Laboratory (No. 2025LABL-B12), and by the National Natural Science Foundation of China (62374031, 62331009), and by NSFC-Jiangsu Province (BK20240173).

<sup>†</sup> Corresponding author(email:230238514@seu.edu.cn).

<sup>1</sup>School of Automation, Southeast University; <sup>2</sup>Nanjing XinDa Institute of Meteorological Science and Technology; <sup>3</sup>Beijing Leninainfo Technology Co., Ltd.; <sup>4</sup>China CEC Engineering Corporation; <sup>5</sup>School of Mathematical Sciences, Tongji University; <sup>6</sup>State Key Laboratory of Virtual Reality Technology and Systems, Beihang University; <sup>7</sup>College of Meteorology and Oceanography, National University of Defense Technology; <sup>8</sup>Key Laboratory of Transportation Meteorology of China Meteorological Administration, Nanjing Innovation Institute for Atmospheric Sciences;

based models such as DiffCast [20], CasCast [21], and MTLDM [22], along with GAN-based methods like FsrGAN [23], have demonstrated improved perceptual quality and probabilistic forecast skill. More recent innovations include simulation-driven convective uncertainty modeling [24], large-model-inspired multi-scale sequence fusion [3], and multi-modal radar-satellite dual-stream frameworks [25]. Despite these advances, generative models typically require tens to hundreds of iterative denoising or generation steps, resulting in inference latencies on the order of several seconds (e.g., DiffCast requires  $\sim 6.3$ s per sample)—far exceeding the sub-second requirements of real-time operational systems. Moreover, achieving accurate and temporally consistent predictions at the 2–3 hour horizon remains challenging even for these sophisticated approaches.

A key but frequently overlooked factor in extended-horizon nowcasting is the influence of underlying terrain on precipitation dynamics [26], [27], [28], [29]. Topographic features such as mountain ranges, valleys, and coastlines create persistent orographic lifting, rain shadow effects, and thermally driven local circulations that fundamentally shape where and how precipitation develops and intensifies. In topographically complex regions such as Xinjiang, which is bordered by the Tianshan and Kunlun mountain ranges, and Southeast China, characterized by the Nanling Mountains and irregular coastlines, ignoring terrain information introduces systematic spatial biases that purely temporal or spectral improvements cannot fully compensate. Incorporating Digital Elevation Model (DEM) data as an auxiliary geographic input provides the model with static orographic context that anchors precipitation predictions to the underlying landscape, yet this approach remains surprisingly underexplored in the existing nowcasting literature.

Meanwhile, the emergence of state space models (SSMs), particularly the Mamba architecture [30], has opened new possibilities for efficient long-range sequence modeling. Unlike Transformers whose self-attention mechanism scales quadratically with sequence length ( $\mathcal{O}(L^2)$ ), Mamba employs a selective state space mechanism that achieves linear complexity ( $\mathcal{O}(L)$ ) while maintaining competitive long-range memory. This property is highly desirable for modeling the temporal evolution of precipitation systems across 0–3 hour sequences comprising dozens of radar frames [31], [32], [33], [34], [35]. However, Mamba’s inherently sequential scan-based processing is better suited for capturing temporal dependencies than for modeling the two-dimensional spatial correlations within individual radar frames. This observation motivates a hybrid design that leverages Mamba for efficient global temporal memory while retaining self-attention for parallel spatial reasoning, thereby combining the complementary strengths of both paradigms.

To address these co-existing challenges, we propose **MambaRain** (see Fig. 1), a novel multi-scale encoder-decoder framework for accurate and efficient 0–3 hour precipitation nowcasting. MambaRain synergistically integrates Mamba’s linear-complexity long-range temporal modeling with self-attention’s parallel spatial reasoning, enhanced by terrain-aware DEM encoding and a spectral loss function that targets the root cause of prediction blurring. Our framework

specifically addresses three co-existing limitations of current methods: (1) the quadratic computational cost of Transformer-based temporal modeling on long sequences, (2) the absence of explicit spatial dependency modeling in Mamba’s sequential processing, and (3) the spatial-domain MSE blurring effect—tackling each with a dedicated, principled design component. The major contributions of this paper are summarized as follows:

- We propose **MambaRain**, a novel multi-scale Mamba-Attention encoder-decoder framework that integrates Mamba’s efficient long-range temporal modeling with self-attention mechanisms and DEM geographic encoding, extending reliable precipitation nowcasting to the challenging 2–3 hour horizon with competitive computational efficiency.
- We introduce **MFormer**, a hybrid Mamba-Transformer block that resolves the complementarity between Mamba’s sequential global temporal memory and self-attention’s parallel spatial dependency modeling, enabling comprehensive multi-scale spatiotemporal representation learning without incurring quadratic complexity overhead.
- We design a **spectral loss function** operating in the Fourier frequency domain to explicitly penalize discrepancies in high-frequency precipitation structures, mitigating the spatial averaging blur effect while preserving fine-scale convective patterns and sharp precipitation boundaries across extended forecast horizons.

## II. METHOD

### A. Formulation of Precipitation Nowcasting

Given a sequence of historical radar observations  $\mathbf{X} = \{\mathbf{x}_1, \mathbf{x}_2, \dots, \mathbf{x}_T\}$  spanning the past 0-1 hour, our goal is to predict future radar reflectivity fields  $\hat{\mathbf{Y}} = \{\hat{\mathbf{y}}_{T+1}, \hat{\mathbf{y}}_{T+2}, \dots, \hat{\mathbf{y}}_{T+K}\}$  for the subsequent 0-3 hour horizon that approximate the ground truth radar sequences  $\mathbf{Y} = \{\mathbf{y}_{T+1}, \mathbf{y}_{T+2}, \dots, \mathbf{y}_{T+K}\}$ . The extended precipitation nowcasting task is formulated as:

$$\hat{\mathbf{Y}} = f_{\theta}(\mathbf{X}), \quad \theta^* = \arg \min_{\theta} \mathbb{E}[\mathcal{L}(f_{\theta}(\mathbf{X}), \mathbf{Y})], \quad (1)$$

where  $f_{\theta}$  is a learnable radar extrapolation function that maps historical observations to future precipitation fields,  $\mathcal{L}$  is a task-specific loss function, and  $K$  represents the number of future time steps corresponding to the 0-3 hour forecasting horizon.

### B. Framework of MambaRain

Fig. 1(a) illustrates the overall architecture of MambaRain, which comprises an encoder-decoder structure with integrated DEM feature encoding for enhanced precipitation nowcasting through multi-scale spatiotemporal modeling.

The encoder consists of four layers: the first two layers use convolutional blocks and downsampling for low-level feature extraction, while the latter two layers incorporate MFormer modules that integrate Mamba blocks for capturing global spatiotemporal dependencies across extended sequences with

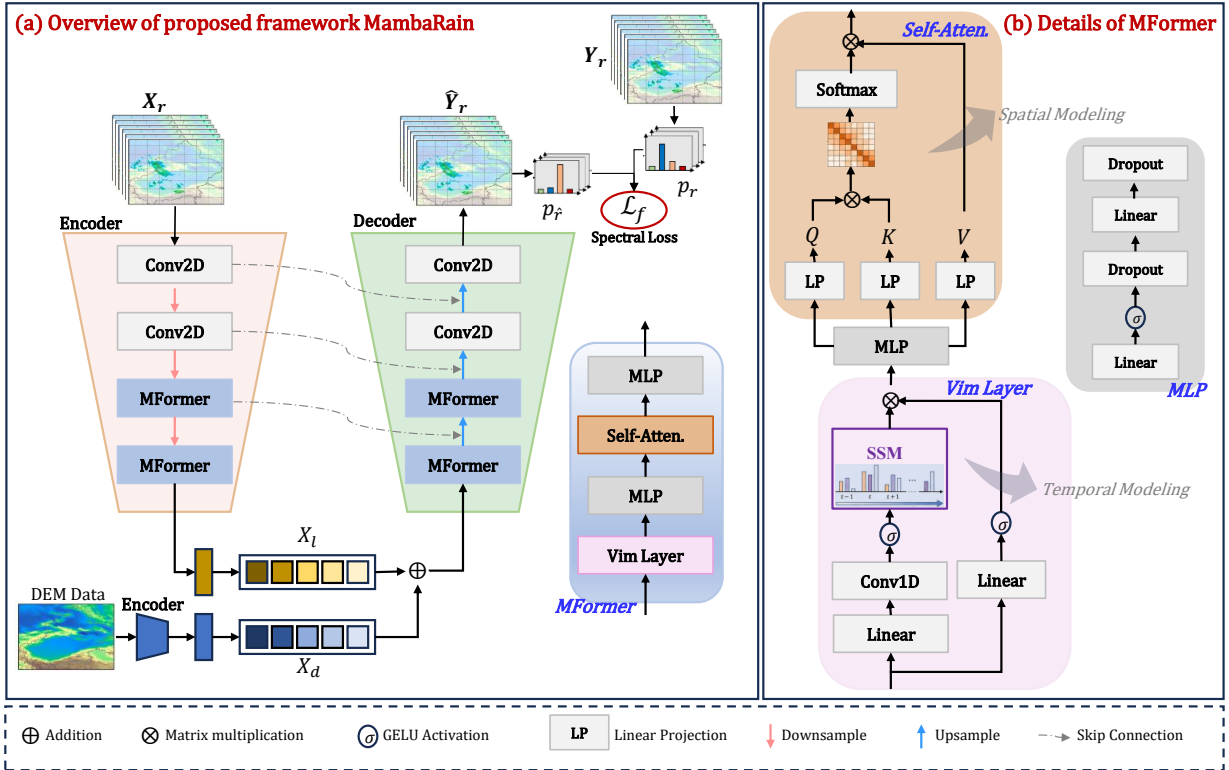


Fig. 1: (a) Overview of the MambaRain model architecture featuring multi-scale encoder-decoder structure with MFormer blocks and DEM integration for terrain-aware precipitation nowcasting. (b) Details of MFormer Block showing the hybrid Mamba-Transformer architecture that combines temporal memory capabilities with spatial attention mechanisms.

self-attention mechanisms for complementary parallel spatial reasoning. The decoder maintains symmetric structure with upsampling operations and MFormer modules in the corresponding layers. Skip connections fuse multi-scale encoder outputs with decoder inputs to preserve low-level features.

DEM geographic information is encoded and integrated at the bottleneck layer for terrain-aware precipitation modeling. The framework employs a spectral loss function to mitigate blur effects and preserve fine-scale motion patterns over the 0-3 hour forecasting horizon.

### C. MFormer Details

The MFormer block represents the core innovation of our framework (see Fig. 1(b)), designed as a hybrid architecture that synergistically integrates Mamba's long-range temporal memory capabilities with self-attention mechanisms for comprehensive spatiotemporal feature extraction.

1) *Feature Integration and Processing Pipeline:* At the encoder's final layer, radar input features are processed to generate output features  $X_l$  with dimensions  $L \times D$ , where  $L$  represents the sequence length and  $D$  denotes the feature dimension. Simultaneously, DEM data undergoes encoding through a dedicated encoder to extract topographic information, followed by tokenization to produce  $X_d$  with compatible dimensions. The integrated features  $X_l + X_d$  serve as input to the decoder's final MFormer layer.

The decoder's output is computed as:

$$\mathbf{X}_{out} = \text{Up}(\text{MFormer}(X_l + X_d)), \quad (2)$$

where the MFormer processing follows a sequential pipeline: MambaVision layer, MLP, self-attention, and final MLP layer, before upsampling.

2) *Selective State Space Mechanism:* The MambaVision component employs a selective state space model (SSM) to capture global spatiotemporal dependencies across extended sequences efficiently. The SSM computation is formulated as:

$$\begin{aligned} h_k &= \bar{A}h_{k-1} + \bar{B}x_k, \\ y_k &= Ch_k + Dx_k, \\ \bar{A} &= e^{A\Delta}, \\ \bar{B} &= (e^{A\Delta} - I)A^{-1}B \approx \Delta B, \end{aligned} \quad (3)$$

where  $B, C \in \mathbb{R}^{D \times N}$  act as projection matrices,  $h_k$  represents the hidden state at step  $k$ , and  $\Delta$  is the discretization parameter. This enables efficient processing of extended sequences with linear computational complexity, providing the temporal memory capabilities essential for extended horizon forecasting.

3) *Self-Attention Mechanism:* Following the MambaVision processing and an intermediate MLP layer, features undergo self-attention computation to enable explicit spatial dependency modeling and parallel global context aggregation. The self-attention mechanism is formulated as:

$$\mathcal{A} = \text{softmax} \left( \frac{\mathbf{Q}\mathbf{K}^T}{\sqrt{d}} \right) \mathbf{V}_l, \quad (4)$$

where  $\mathbf{Q} = \mathbf{X}\mathbf{W}_Q$ ,  $\mathbf{K} = \mathbf{X}\mathbf{W}_K$ ,  $\mathbf{V}_l = \mathbf{X}\mathbf{W}_V$ , and  $\mathbf{W}_Q, \mathbf{W}_K, \mathbf{W}_V$  are learnable weight matrices. The complete MFormer operation is expressed as:

$$\text{MFormer}(X_l + X_d) = \text{MLP}(\mathcal{A}(\text{MLP}(\text{ViM}(X_l + X_d))))), \quad (5)$$

where ViM denotes the MambaVision layer. This sequential processing ensures that Mamba’s sequential temporal processing is complemented by self-attention’s parallel spatial reasoning capabilities, while integrating terrain-aware geographic information with precipitation dynamics.

#### D. Spectral Loss

To address the averaging blur effect in extended precipitation nowcasting, we introduce a spectral loss function that operates in the Fourier frequency domain. Traditional MSE loss optimizes for pixel-wise accuracy, inherently favoring smooth predictions over realistic precipitation boundaries with sharp transitions.

Precipitation systems exhibit frequency-dependent characteristics: high-frequency components encode sharp boundaries and convective structures, while low-frequency components represent large-scale motions. Recent studies [36] have demonstrated that frequency-domain optimization can effectively mitigate spatial averaging effects by preserving spectral characteristics across different scales. We formulate the spectral loss as:

$$\mathcal{L}_{\text{spectral}} = \frac{1}{N} \sum_{n=1}^N \|\mathcal{F}(\hat{\mathbf{y}}_n) - \mathcal{F}(\mathbf{y}_n)\|_2^2 \quad (6)$$

where  $\mathcal{F}(\cdot)$  denotes the 2D FFT,  $\hat{\mathbf{y}}_n$  and  $\mathbf{y}_n$  are predicted and ground truth fields, and  $N$  is the number of samples. This frequency-domain optimization preserves fine-scale motion patterns and maintains global trend consistency over the 0-3 hour horizon.

### III. EXPERIMENTS

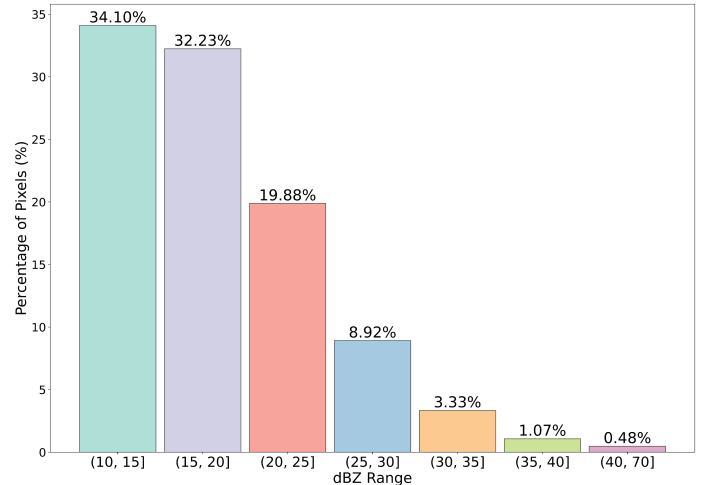
#### A. Implementation Details

**Dataset.** We utilize the SWAN radar dataset from two geographically diverse regions: Xinjiang (73.5°-96.5°E, 34.5°-49.5°N) with mountainous terrain and Southeast China (100°-120°E, 20°-40°N) with varied topography. Both datasets have 0.04° spatial resolution with dimensions of 375×575 and 500×500 respectively (see Fig. 2). Fig. 3 presents the precipitation intensity distribution across both datasets.

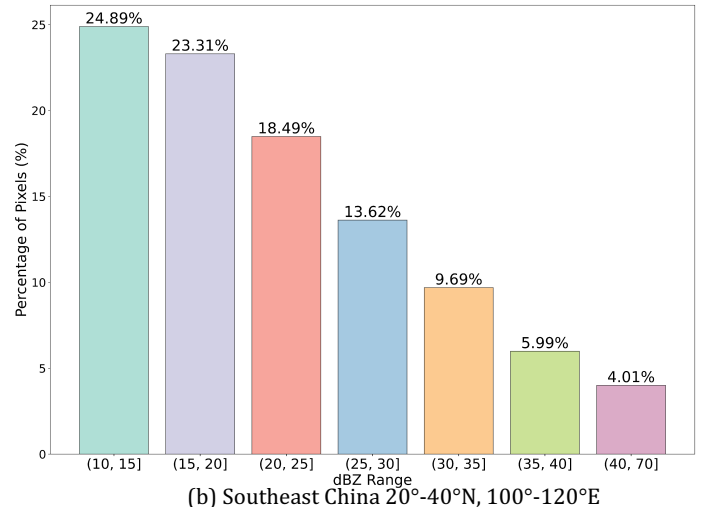


Fig. 2: Study Area

**Training Setup.** MambaRain is trained for 250 epochs with batch size 16 on four NVIDIA RTX 3090 GPUs. The Adam



(a) Xinjiang Province - Northwest China 34.5°-49.5°N, 73.5°-96.5°E



(b) Southeast China 20°-40°N, 100°-120°E

Fig. 3: Echo intensity distribution above 10dBZ for both datasets.

optimizer is used with learning rate 0.0001 and cosine annealing scheduler for stable convergence.

**Evaluation Metrics.** To ensure fair comparison with existing methods, we adopt the same evaluation protocol as FACL [37]. Meteorological forecast skill is assessed using the Critical Success Index (CSI), Equitable Threat Score (ETS), False Alarm Ratio (FAR), and Probability of Detection (POD) at multiple reflectivity thresholds ( $\gamma \geq 10, 15, 20, \text{ and } 30 \text{ dBZ}$ ). These threshold-based metrics are defined using the contingency table elements (hits  $H$ , misses  $M$ , false alarms  $F$ ):

$$\text{CSI} = \frac{H}{H + M + F}, \quad \text{FAR} = \frac{F}{H + F}, \quad \text{POD} = \frac{H}{H + M}. \quad (7)$$

For image quality assessment, we employ the Structural Similarity Index (SSIM), Peak Signal-to-Noise Ratio (PSNR), and Mean Absolute Error (MAE). Perceptual quality is evaluated using Learned Perceptual Image Patch Similarity (LPIPS). All metrics are computed as averages over the full 0-3 hour prediction horizon unless otherwise specified.

**Baseline Comparisons.** We compare MambaRain against representative methods including traditional optical flow approaches (OptFlow) and variational methods (Sprog),

TABLE I: Performance comparison of different models under skill scores on **Southeast China** datasets. The best results are highlighted in bold, and the second-best results are underlined.

Models	Loss	↑ CSI				↑ ETS				↓ FAR				↑ SSIM	↑ PSNR	↓ MAE
		$\gamma \geq 10$	$\gamma \geq 15$	$\gamma \geq 20$	$\gamma \geq 30$	$\gamma \geq 10$	$\gamma \geq 15$	$\gamma \geq 20$	$\gamma \geq 30$	$\gamma \geq 10$	$\gamma \geq 15$	$\gamma \geq 20$	$\gamma \geq 30$			
OptFlow	-	0.548	0.513	0.458	0.342	0.468	0.450	0.418	0.327	0.303	0.329	0.372	0.482	0.692	19.374	0.040
Sprog	-	<u>0.561</u>	<u>0.528</u>	<u>0.471</u>	<u>0.368</u>	0.486	<u>0.467</u>	0.433	<u>0.354</u>	0.266	0.307	0.352	0.446	0.367	12.160	0.270
TrajGRU	MSE	0.557	0.518	0.470	0.339	<u>0.491</u>	0.466	<u>0.438</u>	0.328	<u>0.177</u>	<u>0.192</u>	<u>0.227</u>	<u>0.270</u>	<u>0.734</u>	<u>20.843</u>	<u>0.034</u>
AA-TransUnet	MSE	0.549	0.515	0.466	0.349	0.483	0.463	0.434	0.339	0.182	0.200	0.230	0.289	0.718	20.725	<u>0.034</u>
Earthformer	MSE	0.475	0.428	0.363	0.236	0.406	0.375	0.331	0.226	0.222	0.245	0.295	0.385	0.630	19.182	0.040
MambaUnet	MSE	0.509	0.461	0.412	0.284	0.442	0.409	0.380	0.274	0.190	0.213	0.256	0.310	0.679	20.021	0.037
Diffcast	-	0.459	0.371	0.307	0.245	0.401	0.327	0.266	0.212	0.393	0.525	0.611	0.689	0.387	19.079	2.148
Ours	Spectral Loss	<b>0.619</b>	<b>0.590</b>	<b>0.536</b>	<b>0.418</b>	<b>0.558</b>	<b>0.541</b>	<b>0.505</b>	<b>0.407</b>	<b>0.149</b>	<b>0.169</b>	<b>0.205</b>	<b>0.262</b>	<b>0.788</b>	<b>21.696</b>	<b>0.030</b>

TABLE II: Performance comparison of different models under skill scores on **Xinjiang** datasets. The best results are highlighted in bold, and the second-best results are underlined.

Models	Loss	↑ CSI			↑ ETS			↓ FAR			↑ POD		
		$\gamma \geq 10$	$\gamma \geq 15$	$\gamma \geq 20$	$\gamma \geq 10$	$\gamma \geq 15$	$\gamma \geq 20$	$\gamma \geq 10$	$\gamma \geq 15$	$\gamma \geq 20$	$\gamma \geq 10$	$\gamma \geq 15$	$\gamma \geq 20$
OptFlow	-	0.403	0.343	<u>0.275</u>	0.381	0.328	0.266	0.442	0.505	0.584	<u>0.591</u>	<u>0.529</u>	<u>0.448</u>
Sprog	-	<u>0.453</u>	<u>0.414</u>	<b>0.357</b>	<u>0.434</u>	<u>0.399</u>	<b>0.350</b>	0.364	0.422	0.482	<b>0.611</b>	<b>0.593</b>	<b>0.537</b>
TrajGRU	MSE	0.370	0.328	0.262	0.355	0.318	0.256	0.225	0.274	0.352	0.415	0.375	0.305
AA-TransUnet	MSE	0.371	0.328	0.255	0.356	0.318	0.249	0.223	<u>0.265</u>	0.347	0.415	0.372	0.295
Earthformer	MSE	0.369	0.327	0.195	0.354	0.316	0.191	0.240	0.290	<b>0.325</b>	0.417	0.377	0.216
MambaUnet	MSE	0.329	0.292	0.209	0.315	0.282	0.204	<b>0.200</b>	<b>0.259</b>	0.394	0.358	0.325	0.242
Ours	Spectral Loss	<b>0.464</b>	<b>0.428</b>	<b>0.357</b>	<b>0.449</b>	<b>0.417</b>	<b>0.350</b>	<u>0.220</u>	0.276	<u>0.342</u>	0.537	0.512	0.438

TABLE III: Model parameters comparison on **Southeast China** datasets.

Model	Params (M)	Inference(ms) ↓	CSI( $\gamma \geq 20$ )↑	CSI( $\gamma \geq 30$ )↑
TrajGRU	11.92	3965	0.470	0.339
AA-TransUnet	39.98	448	0.466	0.349
Earthformer	18.05	233	0.363	0.236
MambaUnet	8.97	613	0.412	0.284
Diffcast	50.45	6345	0.307	0.245
Ours	20.36	320	0.536	0.418

ConvRNN-based models (TrajGRU), CNN-Transformer hybrid architectures (AA-TransUnet), meteorology-oriented models (Earthformer), recent Mamba-based networks (MambaUnet [38]), and diffusion-based Diffcast [20].

### B. Comparisons With State-of-the-Art Methods

**Quantitative Results.** Table I presents performance comparisons on the Southeast China dataset. MambaRain consistently achieves superior performance across all meteorological and image quality metrics. Specifically, our method achieves CSI improvements of 11.7%, 14.0%, and 13.6% at 15 dBZ, 20 dBZ, and 30 dBZ thresholds compared to the best-performing baselines, demonstrating substantial gains across the full intensity spectrum. The FAR reductions are particularly notable, averaging approximately 44% relative to Sprog, which indicates that MambaRain produces significantly fewer false alarms while maintaining high detection rates. In terms of image quality, MambaRain attains the highest SSIM (0.788) and PSNR (21.696 dB) with the lowest MAE (0.030), confirming

that our framework preserves both structural fidelity and pixel-level accuracy. The comparison with the generative baseline DiffCast is especially revealing: MambaRain achieves 74.6% higher CSI at  $\gamma \geq 20$  dBZ while reducing MAE by over 98% and delivering approximately 20 $\times$  faster inference. This demonstrates that our deterministic approach with spectral loss can surpass generative methods without the computational burden of iterative denoising processes.

The Xinjiang dataset presents a more challenging evaluation scenario, as precipitation events in this semi-arid mountainous region are characterized by overall weaker echo intensities and sparser occurrence compared to Southeast China. Despite this, as shown in Table II, MambaRain achieves state-of-the-art performance across all CSI and ETS thresholds, outperforming all competing methods including the strong traditional baseline Sprog. An interesting pattern emerges when examining the FAR-POD trade-off: deep learning baselines achieve lower FAR than traditional methods but at the cost of substantially reduced POD, indicating a systematic tendency toward underprediction. MambaRain strikes a better balance between these competing objectives, maintaining competitive FAR while achieving the highest POD among all deep learning methods. This balanced performance is particularly valuable in operational settings where both missed detections and false alarms carry significant costs. We attribute this advantage to the terrain-aware DEM encoding, which effectively anchors precipitation predictions to the region's complex orographic landscape and helps the model distinguish genuine orographic

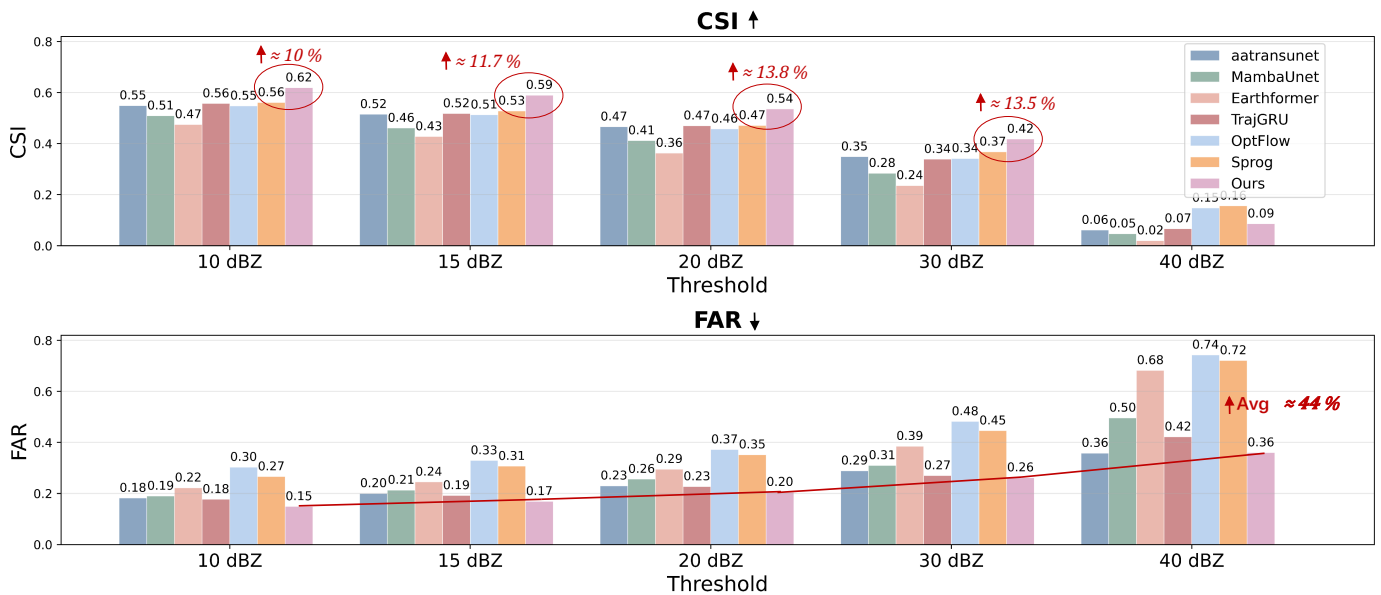


Fig. 4: Threshold-dependent performance comparison of CSI ( $\uparrow$ ) and FAR ( $\downarrow$ ) on the Southeast China dataset. MambaRain achieves consistent CSI improvements of 10–13.8% over the best baseline across all thresholds, while maintaining the lowest FAR on average ( $\approx 44\%$  reduction).

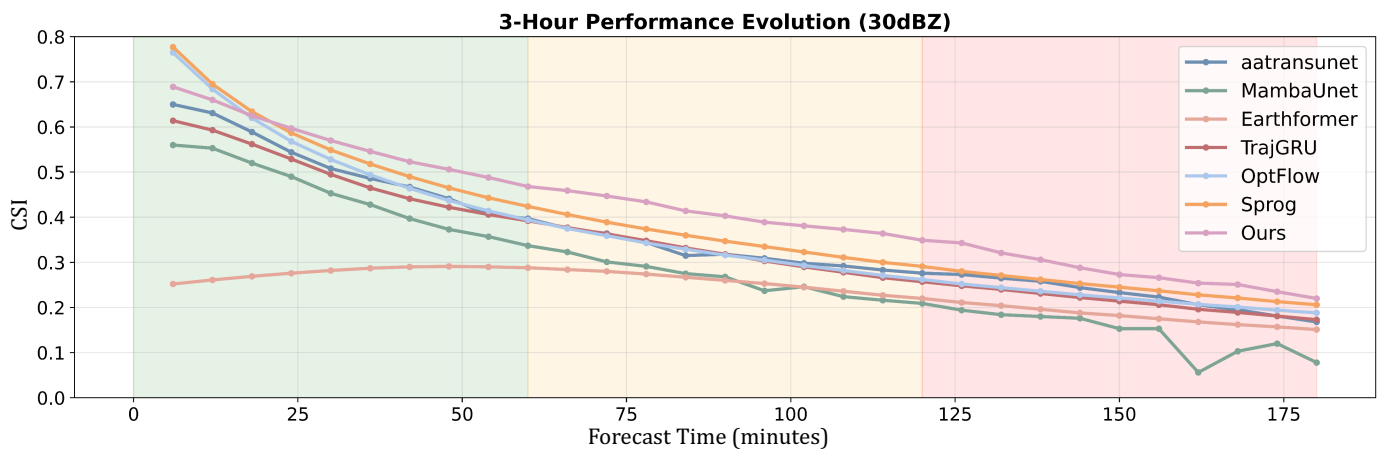


Fig. 5: Temporal evolution of CSI at the 30 dBZ threshold over the 0–3 hour forecasting horizon on the Southeast China dataset. The shaded regions denote short-range (0–50 min), medium-range (50–120 min), and extended-range (120–180 min) forecasting windows, respectively.

enhancement from spurious patterns.

**Computational Efficiency Analysis.** Table III compares model parameters and inference latency across all methods on the Southeast China dataset. MambaRain achieves an inference time of **320 ms** per sample with 20.36M parameters, representing a favorable trade-off between accuracy and efficiency. Compared to DiffCast (50.45M parameters, 6345 ms inference), MambaRain is approximately **20 $\times$**  faster while achieving substantially higher CSI scores (0.536 vs. 0.307 at  $\gamma \geq 20$  dBZ, a **74.6%** improvement). Although Earthformer achieves the fastest inference (233 ms) with fewer parameters (18.05M), its CSI scores are significantly lower (0.363 at  $\gamma \geq 20$  dBZ), indicating that its computational savings come at a considerable accuracy cost. TrajGRU, despite having only 11.92M parameters, requires 3965 ms due to its sequential recurrent processing. MambaRain’s 320 ms latency comfortably meets the real-time operational requirement for

6-minute update cycles, making it practically deployable in meteorological forecasting centers.

**Threshold-Dependent Analysis.** Fig. 4 illustrates CSI and FAR performance across different precipitation intensity thresholds on the Southeast China dataset. MambaRain maintains consistent advantages in both metrics across the entire threshold range from 10 dBZ to 50 dBZ. The most substantial improvements are observed at moderate precipitation intensities (20–30 dBZ), which correspond to light-to-moderate rainfall events that occur most frequently and are critical for practical operational applications. At higher thresholds ( $\geq 40$  dBZ), all methods exhibit performance degradation due to the inherent rarity and high spatial variability of heavy precipitation events, but MambaRain still maintains a noticeable margin in both CSI and FAR over competing approaches, demonstrating its robustness across the full intensity spectrum.

**Temporal Performance Evolution.** Fig. 5 demonstrates our

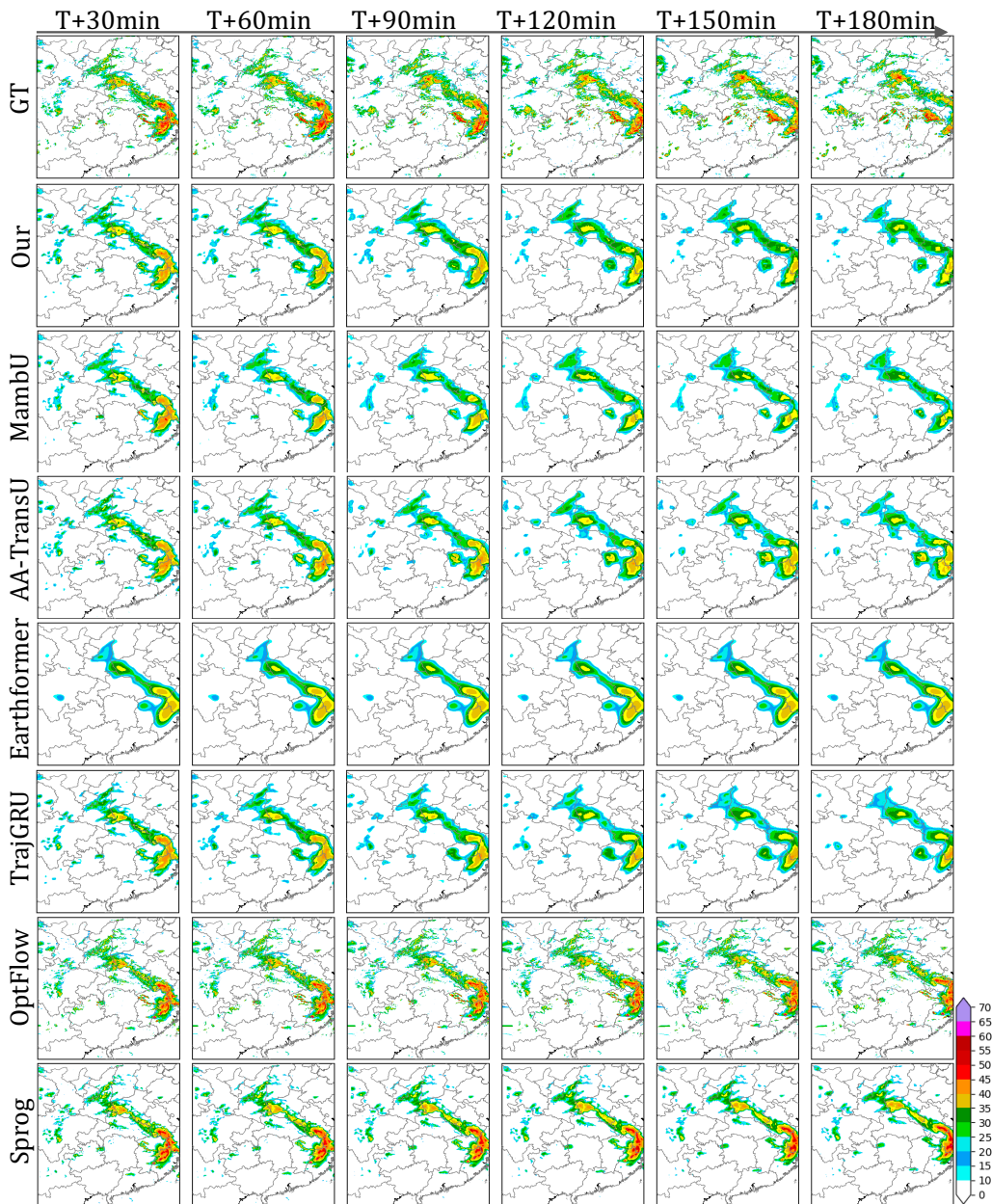


Fig. 6: Visualization comparison of different models results at T+30 to T+180 min on Southeast China dataset. Rows correspond to ground truth and seven competing methods; columns represent increasing forecast lead times.

model's sustained performance advantage throughout the 0-3 hour forecasting horizon. Unlike baseline methods that exhibit rapid performance degradation beyond 90 minutes, MambaRain maintains relatively stable CSI scores, with the 30dBZ threshold analysis revealing superior long-term forecasting capabilities essential for extended nowcasting applications.

**Qualitative Analysis.** Figs. 6 and 7 provide visual comparisons of precipitation forecasts across six time horizons (T+30 min to T+180 min) on the Southeast China and Xinjiang datasets, respectively. On the Southeast China dataset (Fig. 6), traditional methods OptFlow and Sprog produce reasonable spatial structures at short lead times but exhibit severe smoothing artifacts and echo dissipation beyond T+90 min, as their linear motion assumptions fundamentally fail to capture con-

vective initiation and cell merging at extended horizons. Deep learning baselines (TrajGRU, AA-TransUnet, Earthformer, MambaUnet) yield sharper outputs at early time steps but suffer from progressive intensity underestimation driven by the MSE regression-to-the-mean effect, with predicted echo fields fading noticeably by T+120 min. In contrast, MambaRain maintains more realistic precipitation structures with better-retained echo intensities and sharper spatial boundaries throughout the full 3-hour window, directly benefiting from the spectral loss that penalizes high-frequency discrepancies in the Fourier domain. On the Xinjiang dataset (Fig. 7), where overall echo intensities are weaker and precipitation patterns are strongly modulated by complex orography, MambaUnet and AA-TransUnet still exhibit noticeable intensity underes-

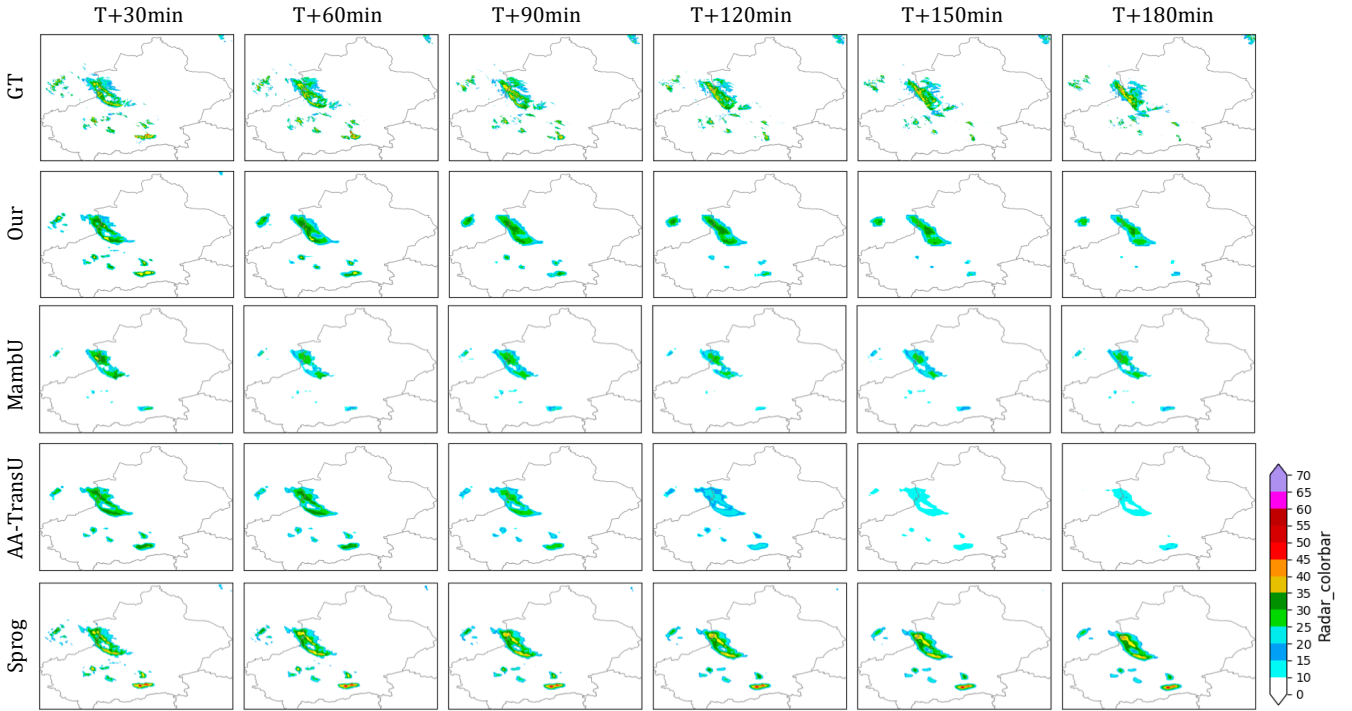


Fig. 7: Visualization comparison of different models results at T+30 to T+180 min on Xinjiang Province dataset. Rows correspond to ground truth and seven competing methods; columns represent increasing forecast lead times.

timation at longer lead times, while Sprog remains relatively competitive at early horizons due to its simple extrapolation mechanism. MambaRain produces spatially coherent forecasts that better preserve orographic precipitation structures along the mountain ranges, demonstrating the practical value of terrain-aware DEM encoding in topographically complex regions.

TABLE IV: Ablation study on the Xinjiang and Southeast China dataset. The best results are highlighted in bold, and the second-best results are underlined.

Block	Data	Loss	Xinjiang		Southeast China	
			Avg.CSI $\uparrow$	Avg.FAR $\downarrow$	Avg.CSI $\uparrow$	Avg.FAR $\downarrow$
$\checkmark$	$\checkmark$	$\times$	0.263	0.383	0.488	0.210
$\checkmark$	$\times$	$\checkmark$	0.288	0.373	0.497	0.213
$\times$	$\checkmark$	$\checkmark$	<u>0.301</u>	<u>0.326</u>	<u>0.507</u>	<u>0.208</u>
$\checkmark$	$\checkmark$	$\checkmark$	<b>0.321</b>	<b>0.314</b>	<b>0.540</b>	<b>0.196</b>

**Ablation Studies.** Table IV presents ablation results on both datasets to validate each proposed component. The full MambaRain configuration consistently achieves the best performance in terms of both CSI and FAR. Removing the MFormer module induces the most severe degradation across both datasets, confirming that the hybrid Mamba-Attention design is the primary contributor to spatiotemporal modeling capability. Replacing the spectral loss with standard MSE leads to a notable CSI drop and increased FAR, validating that frequency-domain supervision is essential for preserving high-frequency precipitation structures at extended lead times. Excluding DEM encoding produces a more pronounced performance penalty on the Xinjiang dataset than on Southeast China, consistent with the expectation that terrain-aware geographic priors are especially critical in orographically complex regions. These results confirm that the three components are

complementary and collectively necessary for achieving state-of-the-art nowcasting performance.

#### IV. CONCLUSION

This paper presents MambaRain, a multi-scale precipitation nowcasting framework for extended 0–3 hour forecasting from ground-based radar remote sensing observations. The proposed MFormer block synergistically combines Mamba’s linear-complexity sequential temporal modeling with self-attention’s parallel spatial reasoning, addressing the complementary limitations of each mechanism when applied independently to spatiotemporal radar data. Terrain-aware DEM encoding is incorporated to mitigate systematic orographic biases in topographically complex regions, and a Fourier-domain spectral loss is introduced to preserve fine-scale precipitation structures against the regression-to-the-mean blurring effect inherent in MSE-optimized deterministic models. Extensive experiments on the geographically diverse Xinjiang and Southeast China SWAN datasets demonstrate that MambaRain consistently outperforms state-of-the-art baselines in both CSI and FAR across the full intensity threshold range, while meeting sub-second operational latency requirements. Ablation studies confirm the complementary contribution of each proposed component to the overall performance gains.

**Limitations and Future Work.** Despite the promising results, the current framework is deterministic and does not quantify forecast uncertainty, and its generalization across heterogeneous radar networks remains to be verified. Future work will focus on further refinement of the proposed architecture, including more fine-grained spatiotemporal representation and improved handling of extreme precipitation at high intensity thresholds.

## REFERENCES

- [1] C. Shi, H. Xu, Y. Li, Y.-L. Wei, Y. Feng, Y. Zhang, and D. Niu, "Wavec2r: Wavelet-driven coarse-to-refined hierarchical learning for radar retrieval," in *Proceedings of the AAAI Conference on Artificial Intelligence*, vol. 40, no. 11, 2026, pp. 8951–8959.
- [2] K. Lin, B. Zhang, D. Yu, W. Feng, S. Chen, F. Gao, X. Li, and Y. Ye, "Alphapre: Amplitude-phase disentanglement model for precipitation nowcasting," in *Proceedings of the Computer Vision and Pattern Recognition Conference*, 2025, pp. 17 841–17 850.
- [3] F. Gao, C. Luo, G. Deng, X. Li, B. Zhang, D. Yu, and Y. Ye, "Lmcast: A pretrained language model guided long-term memory transformer for precipitation nowcasting," *Neural Networks*, p. 108168, 2025.
- [4] D. Yu, W. Du, K. Lin, X. Li, Y. Ye, C. Luo, and X. Chen, "Pimmnet: Introducing multi-modal precipitation nowcasting via a physics-informed perspective," in *Proceedings of the 33rd ACM International Conference on Multimedia*, 2025, pp. 11 522–11 531.
- [5] A. Allen, S. Markou, W. Tebbutt, J. Requeima, W. P. Bruinsma, T. R. Andersson, M. Herzog, N. D. Lane, M. Chantry, J. S. Hosking *et al.*, "End-to-end data-driven weather prediction," *Nature*, vol. 641, no. 8065, pp. 1172–1179, 2025.
- [6] D. Niu, C. Shi, T. Zhang, H. Wang, Z. Zang, M. Jiang, and J. Yang, "M4caster: Multi-source, multi-spatial, multi-temporal modeling for precipitation nowcasting," *Neurocomputing*, vol. 648, p. 130621, 2025.
- [7] P. Chang, D. Fu, X. Liu, F. S. Castruccio, A. F. Prein, G. Danabasoglu, X. Wang, J. Bacmeister, Q. Zhang, N. Rosenbloom *et al.*, "Future extreme precipitation amplified by intensified mesoscale moisture convergence," *Nature Geoscience*, vol. 19, no. 1, pp. 33–41, 2026.
- [8] M. Cui, L. Jia, J. Lu, C. Zheng, and D. Ji, "D-pra: A dynamic two-step real-time precipitation retrieval algorithm based on geostationary satellite observation," *IEEE Transactions on Geoscience and Remote Sensing*, vol. 63, pp. 1–16, 2025.
- [9] Y. Zhang, S. Xiong, H. Wang, W. Yin, J. Peng, Y. Zhang, C. Zhou, H. Chen, Q. Zhao, and P. Duan, "How effective are time-series models for precipitation nowcasting? a comprehensive benchmark for gnss-based precipitation nowcasting," *IEEE Transactions on Geoscience and Remote Sensing*, vol. 64, pp. 1–16, 2026.
- [10] D. Qian, Y. Lyu, Z. Shen, H. Wu, R. Huang, B. Yong, and H. Su, "Detection accuracy of high-resolution infrared satellite precipitation estimates over mainland china: A multiperspective assessment of fengyun-4a," *IEEE Journal of Selected Topics in Applied Earth Observations and Remote Sensing*, vol. 18, pp. 7264–7280, 2025.
- [11] Z. Pan, R. Hang, Q. Liu, C. Shi, Z. Xu, and X.-T. Yuan, "Joint intensity and spatio-temporal representation learning for extreme precipitation nowcasting," *IEEE Journal of Selected Topics in Applied Earth Observations and Remote Sensing*, vol. 18, pp. 18 905–18 921, 2025.
- [12] Z. Wang, B. He, C. Wang, B. Xu, and C. Bai, "Precipitation retrieval integrating multiple satellite observations: A dataset and a framework," *IEEE Transactions on Geoscience and Remote Sensing*, vol. 63, pp. 1–15, 2025.
- [13] C. Zhang, X. Zhou, X. Zhuge, and M. Xu, "Learnable optical flow network for radar echo extrapolation," *IEEE Journal of Selected Topics in Applied Earth Observations and Remote Sensing*, vol. 14, pp. 1260–1266, 2020.
- [14] R. Reinoso-Rondinel, M. Rempel, M. Schultze, and S. Trömel, "Nationwide radar-based precipitation nowcasting—a localization filtering approach and its application for germany," *IEEE Journal of Selected Topics in Applied Earth Observations and Remote Sensing*, vol. 15, pp. 1670–1691, 2022.
- [15] X. Shi, Z. Chen, H. Wang, D. Y. Yeung, W. K. Wong, and W. C. Woo, "Convolutional lstm network: A machine learning approach for precipitation nowcasting," in *Proc. Adv. Neural Inf. Process. Syst. (NeurIPS)*, vol. 28, 2015, pp. 802–810.
- [16] X. Shi, Z. Gao, L. Lausen, H. Wang, D. Y. Yeung, W. K. Wong, and W. C. Woo, "Deep Learning for Precipitation Nowcasting: A Benchmark and A New Model," in *Proc. Adv. Neural Inf. Process. Syst. (NeurIPS)*, 2017, pp. 5617–5627.
- [17] Y. Yang and S. Mehrkanoon, "Aa-transunet: Attention augmented transunet for nowcasting tasks," in *Proc. Int. Joint Conf. Neural Netw. (IJCNN)*, 2022, pp. 01–08.
- [18] Z. Gao, X. Shi, H. Wang, Y. Zhu, Y. B. Wang, M. Li, and D.-Y. Yeung, "Earthformer: Exploring space-time transformers for earth system forecasting," in *Proc. Adv. Neural Inf. Process. Syst. (NeurIPS)*, vol. 35, 2022, pp. 25 390–25 403.
- [19] Y. Zhang, M. Long, K. Chen, L. Xing, R. Jin, M. I. Jordan, and J. Wang, "Skillful nowcasting of extreme precipitation with nowcastnet," *Nature*, vol. 619, no. 7970, pp. 526–532, 2023.
- [20] D. Yu, X. Li, Y. Ye, B. Zhang, C. Luo, K. Dai, R. Wang, and X. Chen, "Diffcast: A unified framework via residual diffusion for precipitation nowcasting," in *Proc. IEEE/CVF Conf. Comput. Vis. Pattern Recognit. (CVPR)*, 2024, pp. 27 758–27 767.
- [21] J. Gong, L. Bai, P. Ye, W. Xu, N. Liu, J. Dai, X. Yang, and W. Ouyang, "Cascast: Skillful high-resolution precipitation nowcasting via cascaded modelling," *arXiv preprint arXiv:2402.04290*, 2024.
- [22] L. Chaorong, L. Xudong, Y. Qiang, Q. Fengqing, and H. Yuanyuan, "Extreme precipitation nowcasting using multi-task latent diffusion models," *IEEE Trans. Geosci. Remote Sens.*, 2024.
- [23] D. Niu, Y. Li, H. Wang, Z. Zang, M. Jiang, X. Chen, and Q. Huang, "FsrGAN: A satellite and radar-based fusion prediction network for precipitation nowcasting," *IEEE J. Sel. Top. Appl. Earth Obs. Remote Sens.*, 2024.
- [24] Y. Yin, S. Chen, Y. Li, L. Wang, R. Jin, W. Cui, and S. Xiang, "Simcast: Enhancing precipitation nowcasting with short-to-long term knowledge distillation," *arXiv preprint arXiv:2510.07953*, 2025.
- [25] K. Xu, J. Gong, W. Zhang, B. Fei, L. Bai, and W. Ouyang, "Syncast: Synergizing contradictions in precipitation nowcasting via diffusion sequential preference optimization," *arXiv preprint arXiv:2510.21847*, 2025.
- [26] Z. Zeng, N. Peleg, H. Chen, and L. Zhuo, "Multifactor spatial downscaling of satellite precipitation based on vegetation index and elevation," *IEEE Journal of Selected Topics in Applied Earth Observations and Remote Sensing*, vol. 19, pp. 3260–3273, 2026.
- [27] Z. Jian, Q. Yang, H. Liu, and J. Shao, "A framework of multi-source precipitation data fusion in the yellow river basin based on climate and terrain partitioning," *IEEE Transactions on Geoscience and Remote Sensing*, pp. 1–1, 2026.
- [28] X. Luo, J. Liao, H. Wang, T. Zhang, Q. Zeng, T. Yu, and Z. Li, "Improving the spatiotemporal resolution of satellite remote sensing precipitation in complex terrain—based on the random forest method," *IEEE Journal of Selected Topics in Applied Earth Observations and Remote Sensing*, vol. 19, pp. 10 687–10 700, 2026.
- [29] H. Chen, R. Cifelli, and V. Chandrasekar, "Resolving the precipitation microphysical variability induced by orographic enhancement in complex terrain over the san francisco bay area," in *IGARSS 2020 - 2020 IEEE International Geoscience and Remote Sensing Symposium*, 2020, pp. 5415–5418.
- [30] A. Gu and T. Dao, "Mamba: Linear-time sequence modeling with selective state spaces," *arXiv preprint arXiv:2312.00752*, 2023.
- [31] S. Zhao, F. Wang, X. Huang, X. Yang, N. Jiang, J. Peng, and Y. Ban, "Mamba-unet: Dual-branch mamba fusion u-net with multiscale spatio-temporal attention for precipitation nowcasting," *IEEE Transactions on Industrial Informatics*, vol. 21, no. 6, pp. 4466–4475, 2025.
- [32] H. Jin, Y. Ye, C. Liu, and F. Gao, "Mambacast: An efficient precipitation nowcasting model with dual-branch mamba," *IEEE Geoscience and Remote Sensing Letters*, vol. 23, pp. 1–5, 2026.
- [33] M. Li, X. Huang, F. Wang, X. Yang, J. Peng, Y. Ban, and N. Jiang, "Adm-unet: An asymmetric dual-branch noncausal mamba u-net with multiscale attention enhancement for cloud mask nowcasting," *IEEE Transactions on Geoscience and Remote Sensing*, vol. 63, pp. 1–15, 2025.
- [34] Y. Wu, Y. Zhu, K. Zhang, J. Qian, J. Xie, and J. Yang, "Weathergen: A unified diverse weather generator for lidar point clouds via spider mamba diffusion," in *2025 IEEE/CVF Conference on Computer Vision and Pattern Recognition (CVPR)*, 2025, pp. 17 019–17 028.
- [35] X. He, J. Li, T. Song, and X. Chen, "Hi-rsmamba: Hierarchical mamba for remote sensing image restoration under adverse weather," *IEEE Journal of Selected Topics in Applied Earth Observations and Remote Sensing*, vol. 19, pp. 7373–7388, 2026.
- [36] Z. Zhao, X. Dong, Y. Wang, J. Wang, Y. Chen, and C. Hu, "MdtNet: Multi-scale deformable transformer network with fourier space losses toward fine-scale spatiotemporal precipitation nowcasting," *IEEE Trans. Geosci. Remote Sens.*, 2024.
- [37] C.-W. Yan, S. Q. Foo, V. H. Trinh, D.-Y. Yeung, K.-H. Wong, and W.-K. Wong, "Fourier amplitude and correlation loss: Beyond using l2 loss for skillful precipitation nowcasting," in *Proc. Adv. Neural Inf. Process. Syst. (NeurIPS)*, vol. 37, 2024, pp. 100 007–100 041.
- [38] J. Liu, H. Yang, H.-Y. Zhou, Y. Xi, L. Yu, C. Li, Y. Liang, G. Shi, Y. Yu, S. Zhang *et al.*, "Swin-umamba: Mamba-based unet with imagenet-based pretraining," in *International conference on medical image computing and computer-assisted intervention*. Springer, 2024, pp. 615–625.